Eidgenössische Technische Hochschule Zürich
Swiss Federal Institute of Technology Zurich

SED
Schweizerischer Erdbebendienst
Swiss Seismological Service

Report on site characterization

Wallhausen, Germany (WALHA)

Poggi Valerio, Manel Hobiger, Donat Fäh

Last modified - 23 / 12 / 2014

1. Introduction

In the framework of the NAGRA seismic network project, an array measurement of the ambient vibration wave-field was performed at the location of the SED station WALHA (Wallhausen, Germany). The scope of the survey is the seismic characterization of the area surrounding the installation (**Figure 1**), which consists in a broadband seismometer (Trillium Compact) with a high-resolution digitizer (Taurus 24Bit @200sps). Ambient vibration analysis has been used to infer the characteristics of the underground structure of the site, with special regard to the one-dimensional shear-wave velocity. Such profile was later used to assess the local seismic response of the station.

For the analysis, different spectral analysis techniques were implemented, consisting in both single and array methods, which are listed below:

- Time-frequency wavelet analysis
- Power-spectral density estimation
- Conventional horizontal to vertical spectral ratios
- Directional horizontal to vertical spectral ratios
- Wavelet polarization analysis
- Three-component high-resolution f-k analysis.

The results of all these analyses conformed to the definition of the final velocity model. In the following, the main results of these investigations are summarized and a final interpretation of the velocity profile is given. From this interpretation, engineering parameters are finally derived, e.g. the Qwl-Vs average velocity, VsZ (including Vs30) and the seismic amplification from the analytical SH-transfer function of the one-dimensional soil column.

2. Survey description

To characterize the seismic response of the site, an array measurement of ambient vibration was performed on 24/06/2014 (**Figure 1**). The array consists of two measuring configurations (A1 and A2) of 14 sensors each and increasing diameter of about 100m and 200m respectively. The two configurations were planned to partially overlap, by sharing 9 common sensors, with the aim of providing a continuous frequency resolution between the two geometries. Configuration A1 recorded for a total of 1h10m, while configuration A2 for 1h40m. The differences in the recording length are due to the different resolution characteristics of the two geometries. As a general rule, larger arrays require longer recording time to produce a reasonable statistics of the ambient vibration processing results. In this case, however, due to an unfortunate presence of transient disturbances, the usable signal length for configuration A2 was reduced to about 1h only. Satisfactory results were nevertheless obtained from the analysis of the two geometries.

High velocities and relatively shallow geophysical bedrock (undeep marine Molasse) were expected for the site. This justifies the use of a large geometry for the array to be successful. The maximum aperture of the array was again controlled by the available space on the hilltop, which was quite flat over the measuring area, but limited toward North-East and South-West from dipping slopes and forests. A precise prior estimation of the possible maximum resolved depth was not possible, due to the large uncertainty of the bedrock velocity, but resolution down to about 110~150m depth was expected.

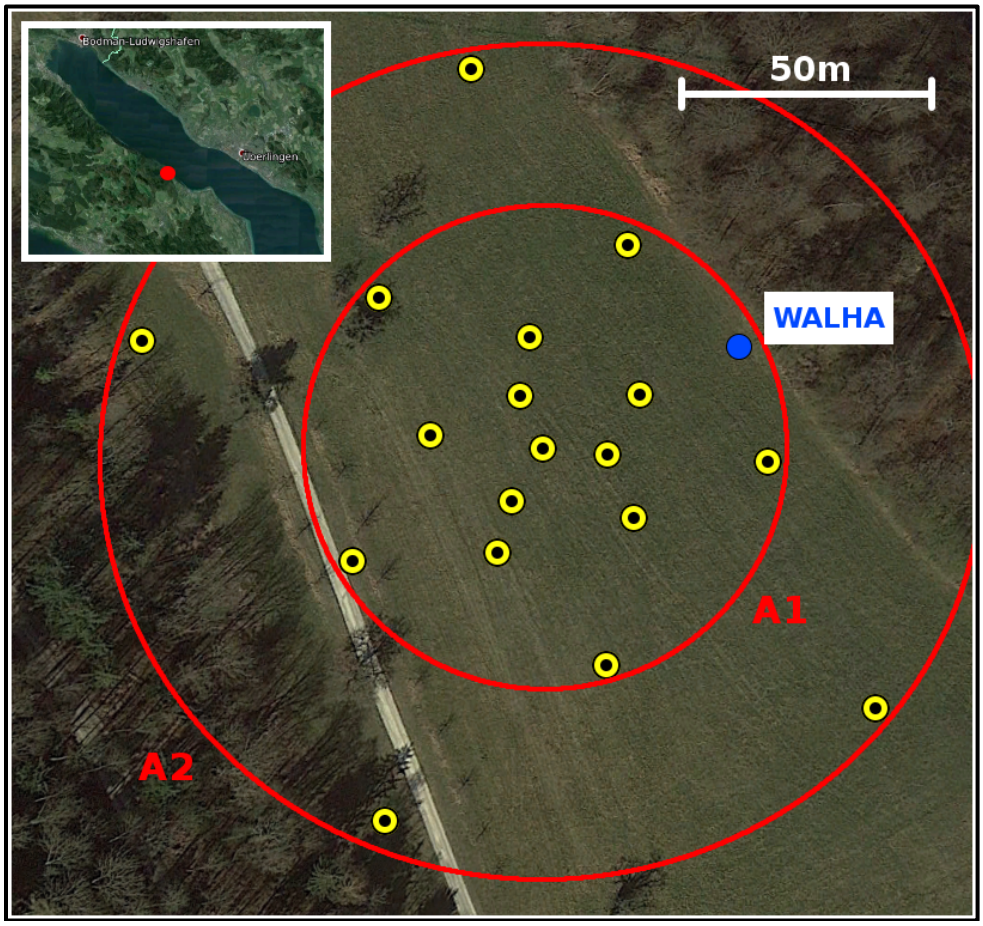

Figure 1 - *Location of the ambient vibration array survey performed in Wallhausen, (SED station WALHA) on 24/06/2014. Two concentric configurations of increasing diameter were implemented (name A1 and A2). Location of the permanent station is shown in blue.*

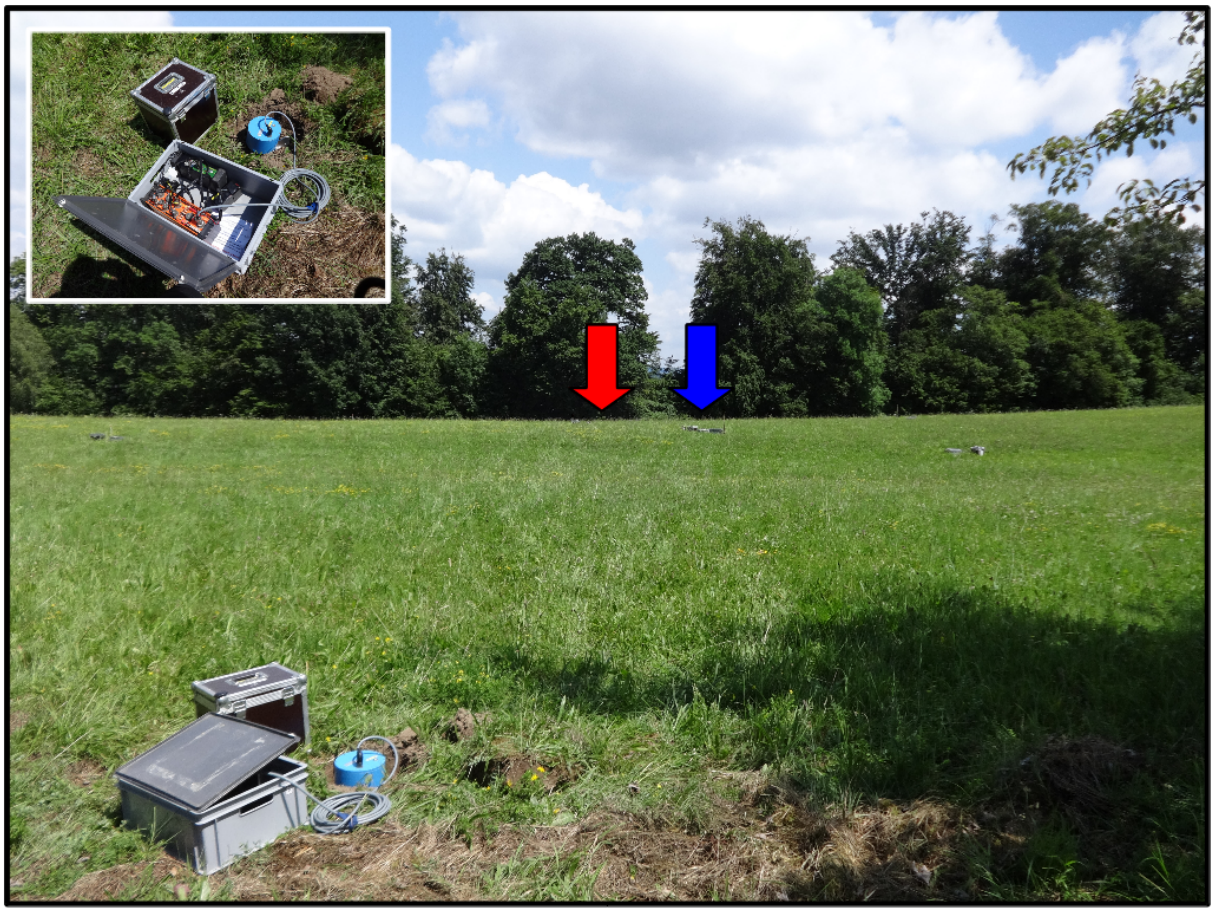

Figure 2 - *Overview of the measurement area. Location of the array central station and of the permanent station WALHA (at the edge of the grass field, close to the forest border) are indicated with blue and red arrows respectively.*

3. Soil type, topography and geology

The array has been set in open field conditions, in a rural area (**Figure 1**, **Figure 2**). The influence of buildings and anthropogenic disturbances is virtually negligible, even though some monochromatic harmonic signals affected the second half of the survey (while recording with array configuration A2). Array sensors have been deployed on free soil. Good coupling with the ground was assured by means of digging small holes at the sensor's places, and by using a special support (*Trihedron*®) that facilitates the leveling of the device even for difficult soil conditions. The measurement area was located on a nearly flat area, just little dipping toward NE. However, no topographic correction has been taken into account before processing.

From the geological points of view (**Figure 3**), the target area is located on a small hill on the Molasse basin (precisely undeep marine Molasse). The surface morphology is considerably smooth and modeled by the action of glaciers during the Pleistocene. The measuring area is visibly surrounded by moranic deposits, clearly identifiable from the surface morphology and confirmed by the geological map of the area. The Molassic bedrock is likely very shallow at the measuring location, but never exposed across the area (a variable-thick cover of quaternary material is generally present). The bedrock probably consists of marl and consolidated sandstone with layers of different texture and granulometry, from very fine sand and silt to occasionally conglomerate. Such site can be classified as of rock ground-type A.

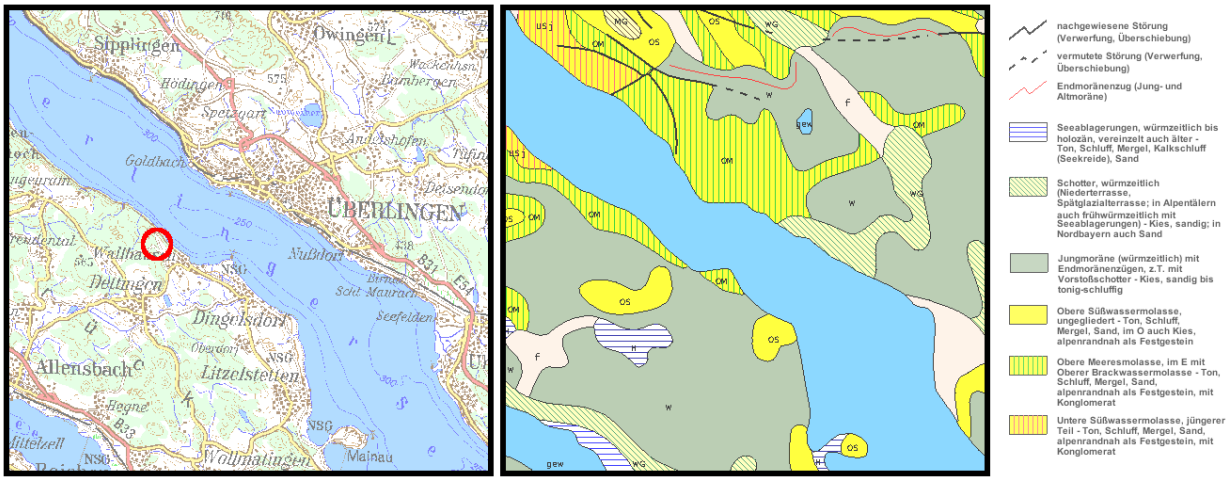

Figure 3 - *Geological map of the lake Constance, in the surroundings of Wallhausen (reproduced from GeoFachdatenAtlas, Bodeninformationssystem Bayern, modified). In red the approximate location of the permanent station WALHA.*

4. Acquisition equipment

Each acquisition point within the array consisted of a three components seismometer (Lennartz 3C with 5s eigenperiod) and a 24 bit data logger (Quanterra Q330). Synchronization between stations was assured by standard GPS, while a more accurate differential GPS (Leica Viva system) was used to precisely locate the sensor's coordinates with a tolerance of less than 5cm.

5. Weather conditions

The weather conditions were optimal and stable during the whole measurement, with no precipitations, no wind and an average (over the whole day) temperature of 16 degrees. Soil was nevertheless most likely saturated from precipitations occurred during the days preceding the survey.

6. Pre-processing and preliminary data-quality control

The three-component recording has been filtered prior to analysis using a band-pass 6th order causal Butterworth filter with corners at 0.2Hz and 50Hz. Although it is not a strict requirement for spectral analysis techniques, such filtering was applied in order to facilitate the preliminary visual inspection of the noise traces and to evaluate the coherency of the wave-field (**Figure 4**). Such procedure gives essential information for the subsequent interpretation of the f-k analysis results.

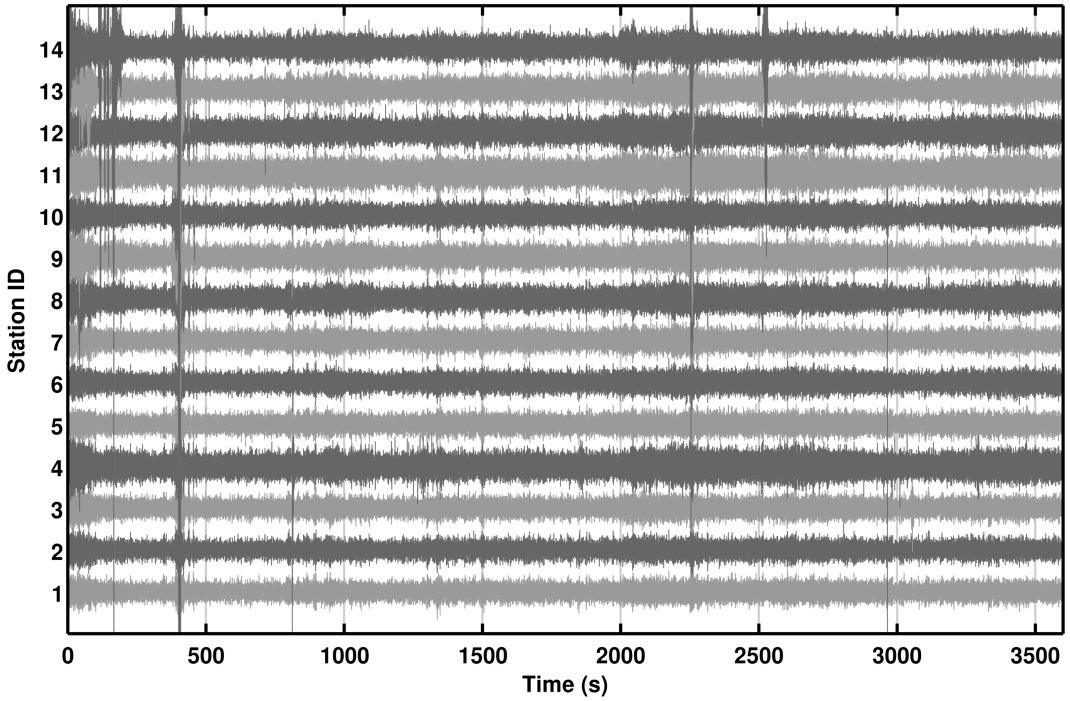

Figure 4 - *Inspection of the useful part of the ambient vibration recording of the Wallhausen array (in this example configuration A1). No strong transients were present during the acquisition, which resulted in an overall good quality of the recordings.*

To assess the quality of the ambient vibration recordings, spectral analysis was subsequently performed. Because of the stochastic nature of the ambient vibration wave-field, a statistical approach has to be used, such as the estimation of the power spectral density (*PSD*). This approach is useful to evaluate the average energy level of the recordings in the analyzed frequency range, and to access the presence of spurious spectral peaks, which might be related to human activity (machinery, pumps). By inspecting the PSD of all the three-component recordings of the array in the range between 0.5 and 40Hz, it is found that the average energy level of the spectrum is overall very low, well within the minimum and maximum bounds of the USGS noise model.

Two spurious peaks have been identified at about 5Hz and 7Hz. Such peaks - very narrow - were nevertheless present only for configuration A2, and did not affect the recordings of configuration A1 (**Figure 5**). This gives a confirmation of their anthropogenic origin (likely a nearby farm). Such harmonic contributions are therefore rejected from any subsequent interpretation.

A1)

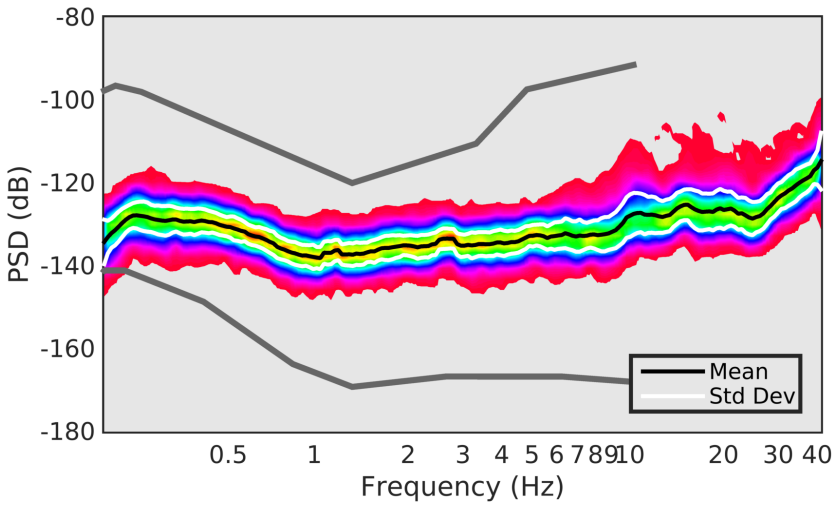

A2)

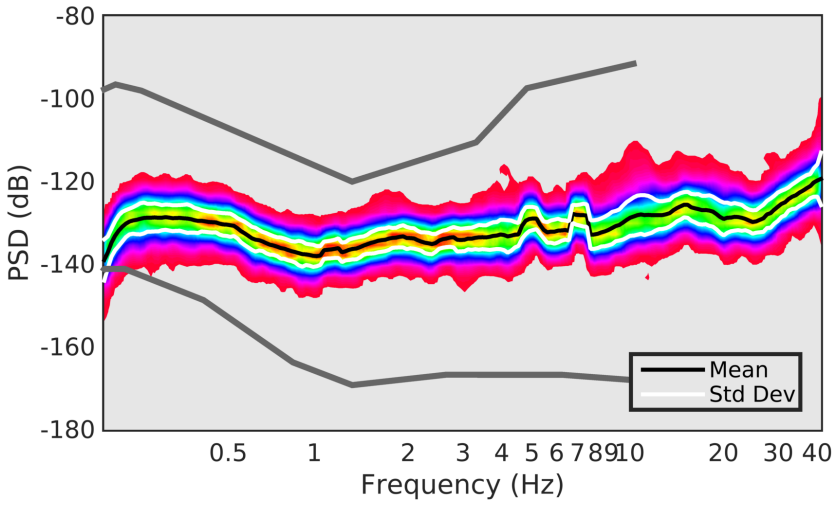

Figure 5 - *Power spectral density (PSD) computed for 1h recording at the central station (WAL002) of the array configuration A1 (top) and A2 (bottom). Similar results were obtained from the other stations of the array. In gray lines are the minimum and the maximum bounds of the USGS noise model, for comparison.*

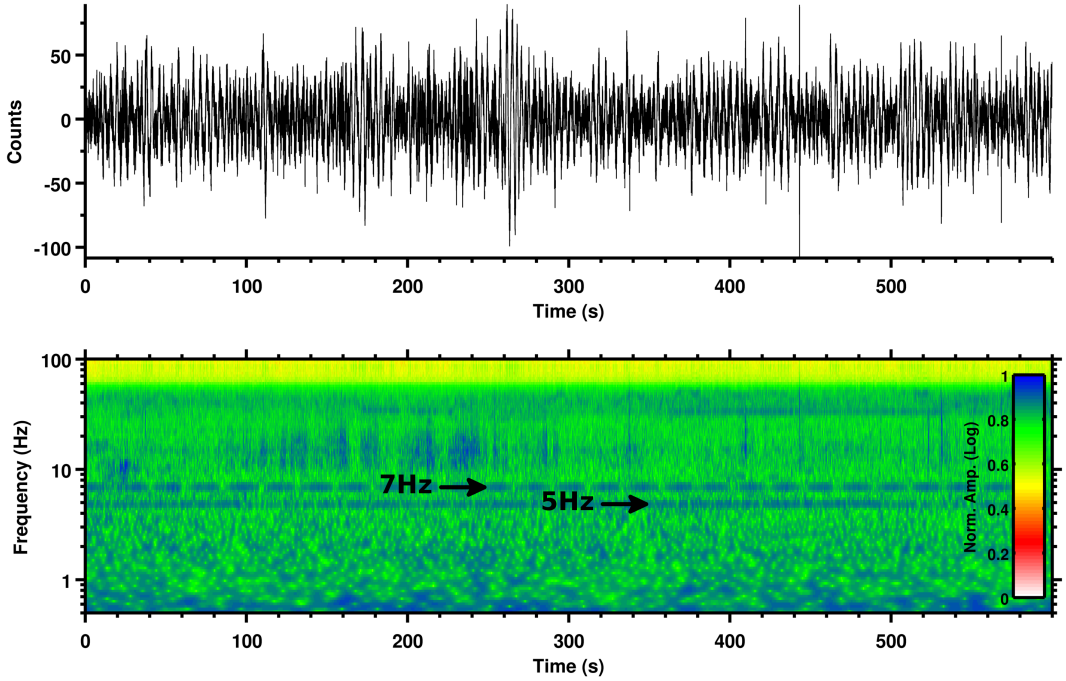

Figure 6 - *Example of spectrogram from 600s of recording of the central station (WAL002) of the array configuration A2. Two harmonic disturbances are visible on the whole spectrogram, at about 5 and 7Hz. These signals were not present during the recordings of configuration A1. For the analysis, the cosine wavelet is used (wavelet parameter = 12).*

Complementary to the aforementioned statistical methods, a spectral decomposition approach is more suitable to assess the stationarity of the ambient vibration wave-field over time. The wavelet time-frequency analysis was then performed over the whole recording time. From such analysis (**Figure 6**) an overall stability of the ambient-vibration wave-field over time is evident. The disturbances at about 5Hz and 7Hz are confirmed to be a nearly harmonic contribution, steady over the whole recording window. This provides a further confirmation of their anthropogenic origin. These disturbances are nevertheless very weak and well localized in frequency; therefore they won't affect the subsequent processing steps.

7. Conventional H/V spectral ratios

The horizontal-to-vertical (H/V) Fourier spectral ratio is a technique widely used in seismic site characterization because of its ability to provide an estimate of the SH wave fundamental frequency of resonance (f_0) of the site. Other than that, H/V ratios are useful to provide information on the Rayleigh wave ellipticity function, which can be used in surface wave dispersion inversion procedures to constrain large velocity contrasts at depth. In this study, we use the H/V technique also to map the variability of the subsoil structure along the investigated area; this is necessary to verify the fulfillment of the 1D structure assumption, which is necessary for the f-k method applied later.

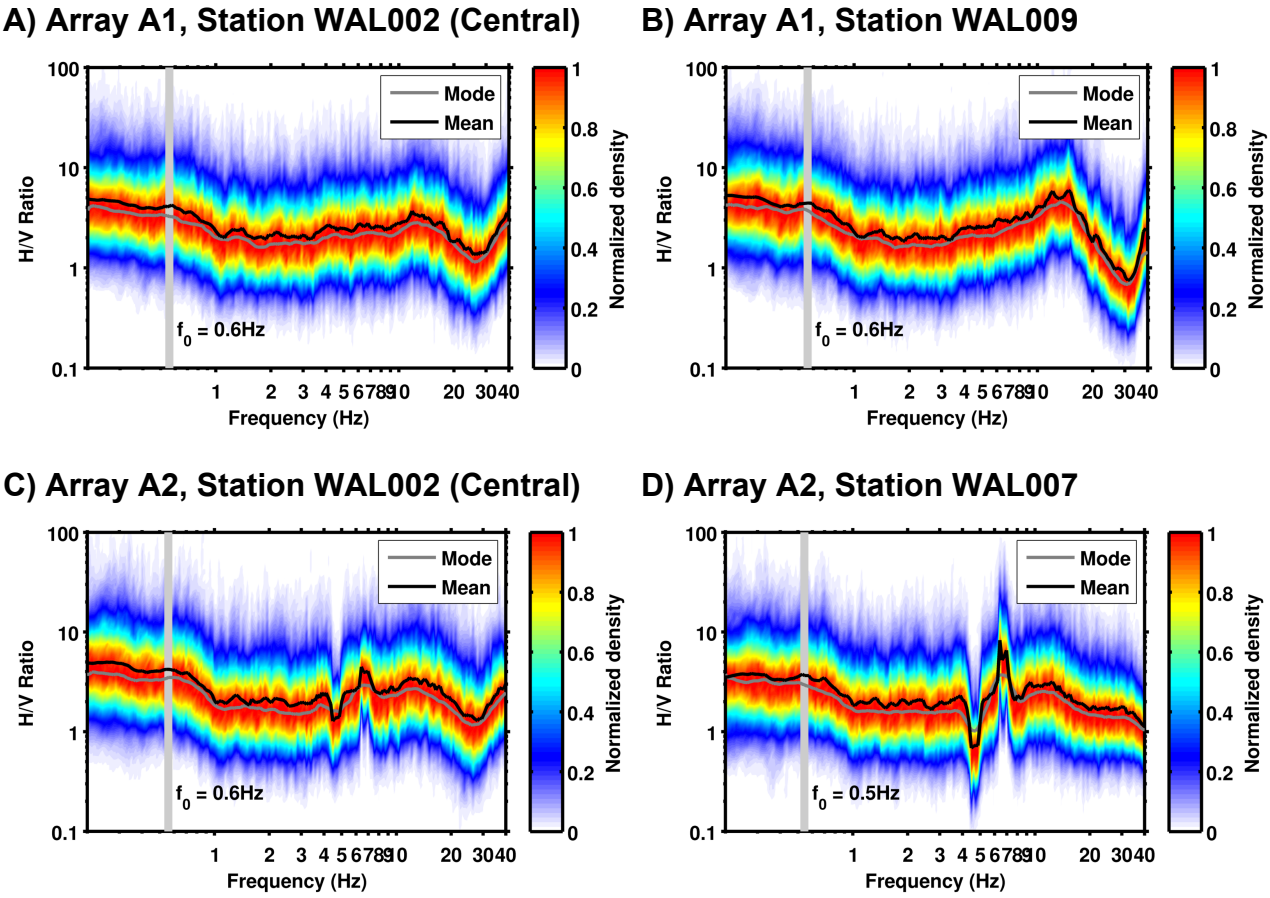

Figure 7 - *Example of H/V spectral ratios for the two concentric configurations A1 and A2. The presence of anthropogenic signals is quite evident in all stations of A2. The resonance frequency of the soil cover, indicated with a light gray line, is due to a lithology change within rock. The additional resonance peak at about 14Hz is likely due to a velocity contrast between topmost soil and underlying rock.*

H/V spectral ratios have been computed for all the recordings at each station of the array and separately for configurations A1 and A2 (e.g. **Figure 7**). The shape of the computed H/V curves is typical of stiff-soil/rock velocity profiles whereas the soil thickness is rather small. The behavior of the noise wave-field at the different stations location is very comparable (**Figure 8**). A relatively small peak is visible at low frequency (around 0.56Hz), quite stable over the whole measuring area. Such maximum is likely induced by a change in lithology at depth, which causes a modest contrast of seismic impedance. The peak should be regarded as the fundamental resonance frequency of the site. Above this frequency, H/V curves are quite flat till about 10~12Hz, with a stable amplitude slightly above 2. At higher frequencies the variability of H/V curves reflects the variability of the topmost part of the ground structure. A second maximum can be observed between about 12Hz and 25Hz. This peak is likely induced by the Quaternary soil cover, which can be very heterogeneous over the measuring area. Interesting to notice how the two previously identified anthropogenic disturbances show a different behavior on H/V ratios (e.g. **Figure 7**C and D). This means, the harmonic signal at 5Hz is mostly vertically polarized, while that one at 7Hz is more pronounced on the horizontal components.

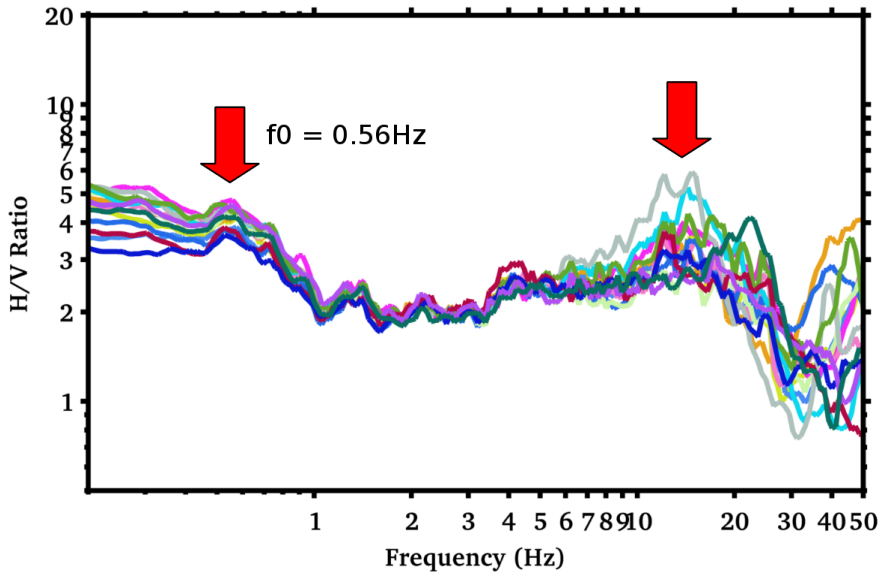

Figure 8 - *Comparison of the H/V spectral ratio curves of all the stations of the array (in this example for the array configuration A1). The curves are stable up to at least 10Hz, confirming the lateral homogeneity of the underlying bedrock velocity structure of the site. A low frequency peak is visible at about 0.56Hz. At high frequencies the spectral ratios are variable across the array. This reflects the complex geometry of the quaternary sediments cover.*

8. Directional analysis

The computation of directional H/V spectral ratio or polarization analysis is useful to reveal asymmetries in the ambient vibration wave-field. Different effects can induce such a behavior: 2D/3D structure, topographic effects or a non-homogeneous distribution of the noise sources. If a strong directionality is found by the analysis, it is generally recommended to carry out further investigations to properly address the origin of polarization.

By processing the directional H/V ratios at all the recording stations of the array (e.g. **Figure 9**) it is possible to observe an overall isotropy of the wave-field in the intermediate frequency range, roughly between 1 and 10Hz. However, the resonance peak at about 0.56Hz has surprisingly a stable directionality of nearly 50°N. The reason for such behavior is nevertheless not clear. This might be induced by the geometry of the hill, which has major axis in the orthogonal direction. At high frequencies, the variability of the H/V peak observed in **Figure 8** is noticeable also in its directionality (not shown here). As already introduced, this can be explained by the variability of the uppermost soil cover layer over the study area and will not be further discussed. It is interesting to notice the directionality of the two previously found harmonic signals which affect the recordings of configuration A2. These maxima are roughly aligned towards NW-SE direction (120~140°N).

The results of the H/V directional analysis are also confirmed by applying the wavelet polarization analysis techniques as described in Burjanek et al. (2008). Also in this case no sign of significant directionality (**Figure 10**A) and polarization (**Figure 10**B) of the wave-field is observable in the frequency band useful for f-k processing. Similarly, the low frequency resonance peak shows directionality similar to that found with H/V analysis, plus a moderate elliptical polarization.

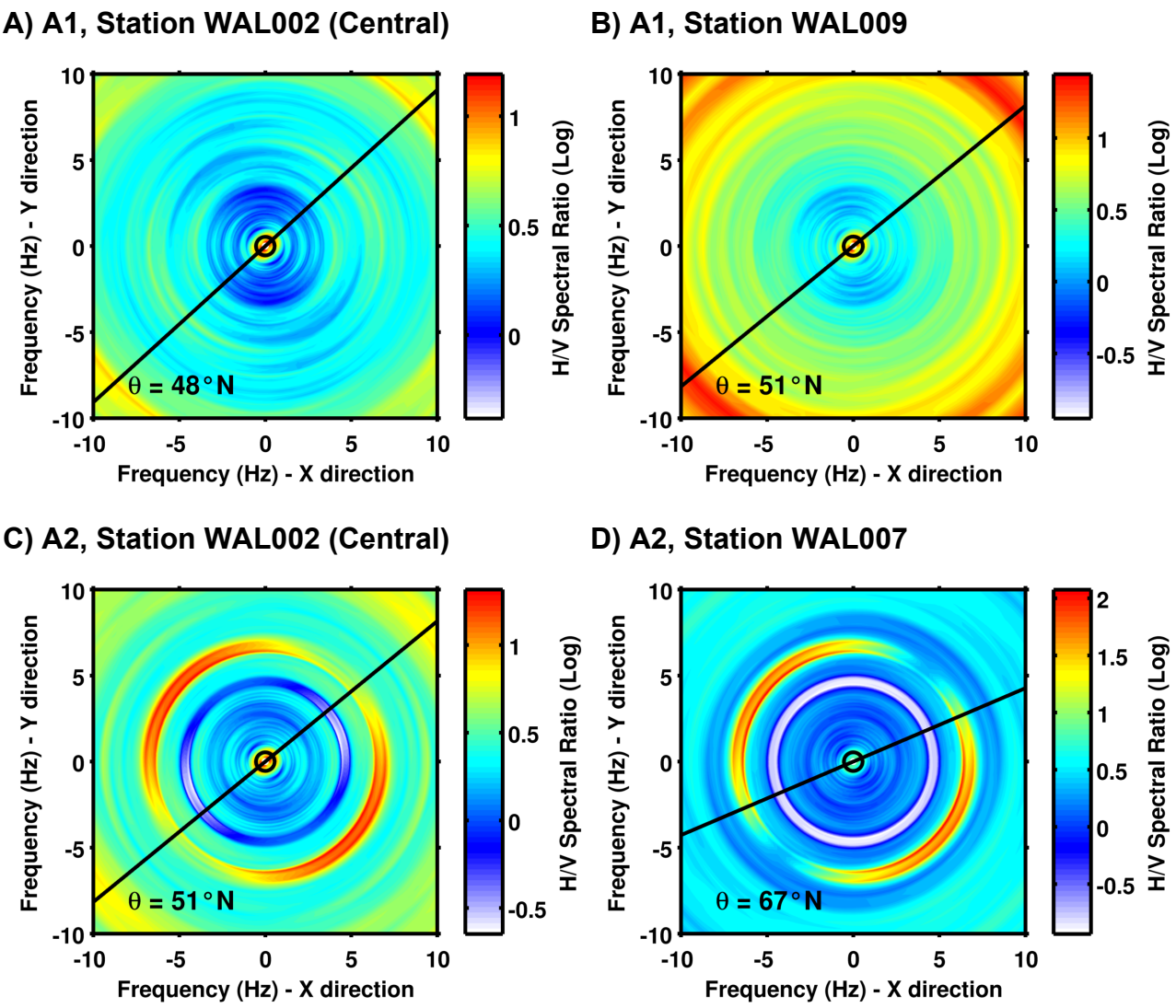

Figure 9 - *Example of directional H/V spectral ratios for the two concentric configurations A1 and A2. No consistent evidence of wave-field anisotropy is present in the intermediate frequency range (1-10Hz), while the low frequency resonance peak (f_0) is preferentially aligned perpendicularly to the hill major axis. Moreover, a strong directionality of the two harmonic disturbances (at 5Hz and 7Hz) is visible on the recordings of array configuration A2.*

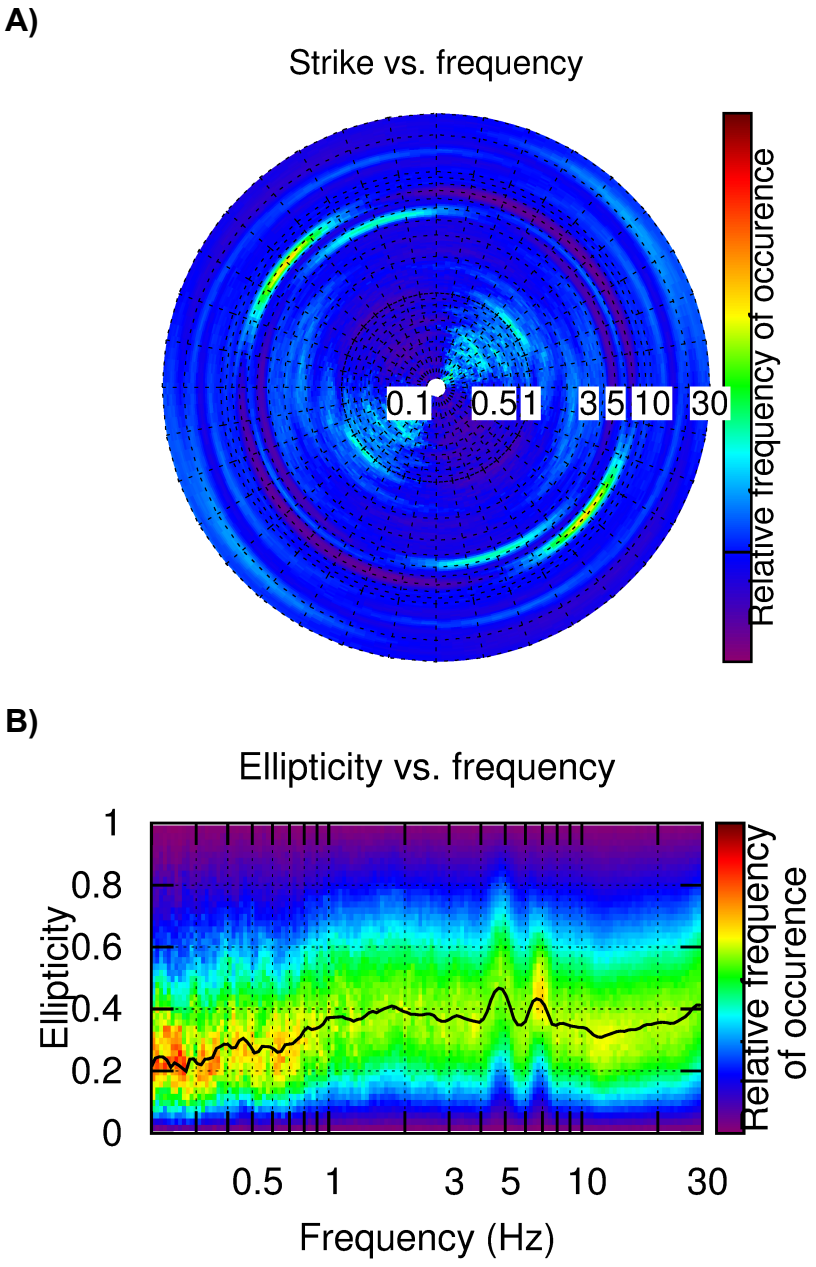

Figure 10 - *Wavelet-based polarization analysis at the central station of the array configuration A2. By analyzing the polarization over strike (A) and the particle motion ellipticity plot (B), no directional effect is visible in the frequency range of interest (roughly 1-10Hz), with the exception of the two anthropogenic disturbances, which are strongly directional.*

9. Three-component f-k analysis

The frequency-wavenumber analysis is a spectral technique based on seismic array recordings that allows retrieving direction and dispersion characteristics of the surface waves. We apply this technique to three-component ambient vibration recordings using a modification of the high-resolution method of Capon (1969) as described in Poggi et al. (2010). Using all the three-components of motion gives the possibility to retrieve information about the propagation of the Rayleigh waves (vertical and radial processing direction) as well as of the Love waves (transversal direction).

As in the case of the previous methods, the ambient vibration recordings are treated statistically by subdividing the traces in sub-windows. For each consecutive window a separated f-k analysis is performed, and the results are then averaged over the whole recording, increasing the robustness of the final estimation.

A) 2-4Hz

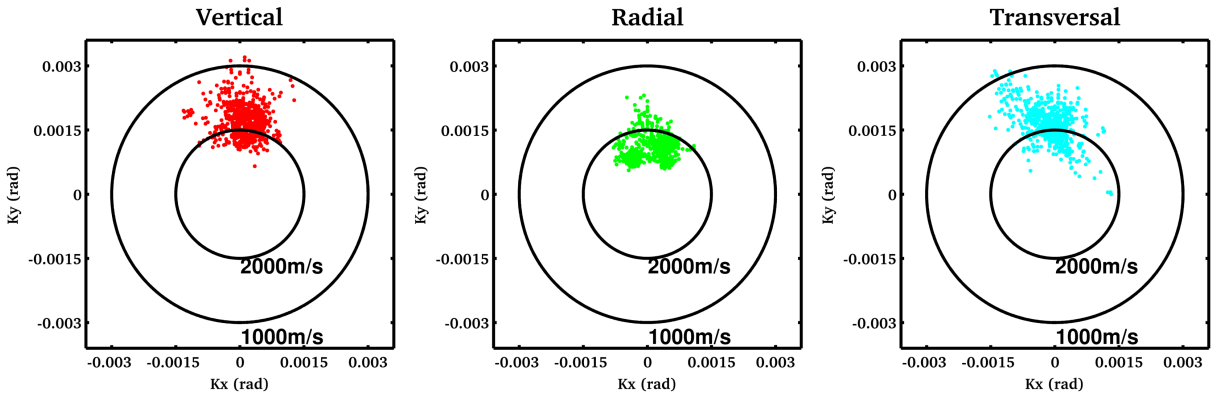

B) 4-8Hz

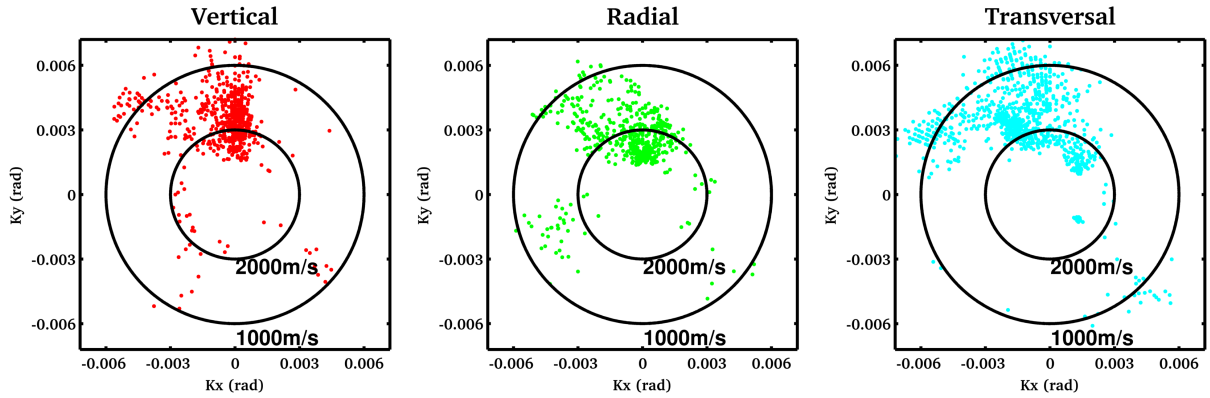

Figure 11 - *Example of distribution of noise sources in the low (2-4Hz) and intermediate frequency range (4-8Hz) obtained from three-component f-k analysis. The source distribution is strongly directional for all the propagation components.*

As first step, from the f-k analysis it is possible to assess the noise source azimuthal distribution over different ranges of frequencies (e.g. **Figure 11**) separately for the vertical, the radial and the transversal direction of polarization. From the analysis of the two geometries A1 and A2, source distribution appears to be strongly directional (anisotropic) in all the components, with major contribution from North. This condition is surprisingly rather stable on the whole analyzed frequency range, but has no direct explanation in terms of settlement location or local geomorphology.

As a second step, the surface-wave dispersion curves are extracted by visual inspection and manual picking of the f-k density plots (**Figure 12** and **Figure 13**), separately for the three polarization direction. Similar, but not identical results have been obtained for the two array configurations. In particular, Love wave dispersion can be well tracked in a broad frequency range (from 3~4Hz to about 20Hz) from both A1 and A2; velocity estimates are also consistent between the two geometries. Rayleigh wave dispersion is of more difficult to interpret. The vertical component shows indications of two modes, whose interpretation is quite clear on A2 (fundamental plus first higher mode), but doubtful on A1. Moreover, Rayleigh velocities are slightly mismatching between the two arrays configurations. This might be induced by the proximity of the two modes and the relatively high velocities of propagation, which can produce biased results especially when using small geometries. For this reason, the final interpretation of Rayleigh modal pattern is mostly based on the results from A2. Complementary, radial component processing confirms the presence of the first higher mode of Rayleigh waves, extending it to lower frequencies and higher velocities.

A summary of all the identified modes from vertical, radial and transversal direction of propagation is presented in **Figure 14**, while the final interpretation of Rayleigh and Love wave dispersion pattern is in **Figure 15**. The dispersion pattern is typical for a gradient velocity profile, with progressive decrease of velocity with increasing frequency.

10. Inversion of the dispersion curves

The surface wave dispersion curves (Rayleigh and Love) obtained from the three-component f-k analysis of the ambient vibrations are inverted to obtain an estimation of the velocity profile of the site (mainly S-wave velocity as function of depth, and to a lesser extend the P-wave velocity, due to the lower sensitivity). The analysis is performed using the software *Dinver* (www.geopsy.org), which implements a direct search approach (**Figure 16**) based on a conditional version of the neighborhood algorithm (Sambridge, 1999).

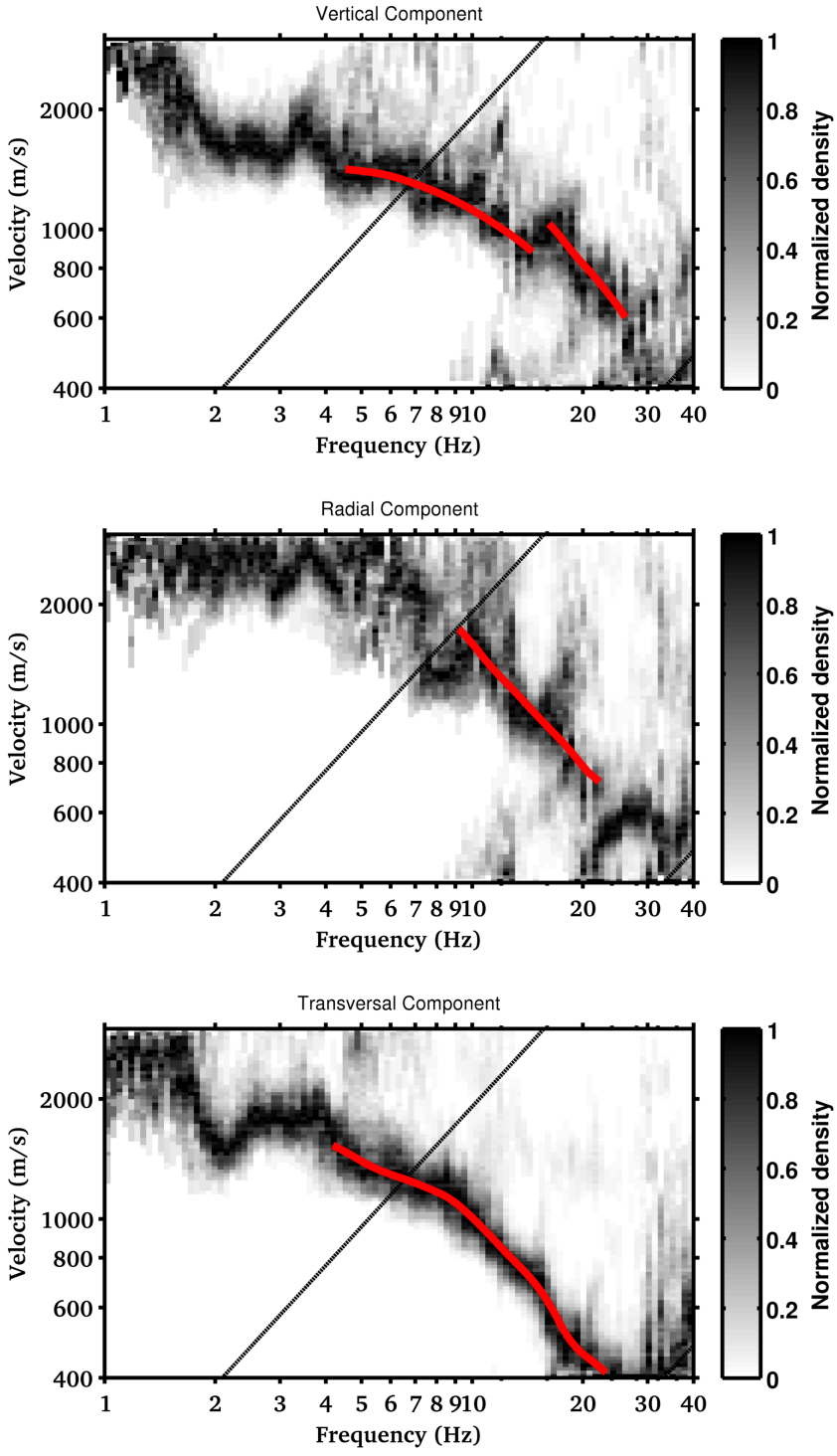

Figure 12 - *Density distribution of the surface wave signals obtained from the recording of the array configuration A1 using three-component f-k analysis. From top to bottom: Rayleigh vertical, Rayleigh radial and Love wave dispersion. In red the interpreted dispersion curves are given (manually selected).*

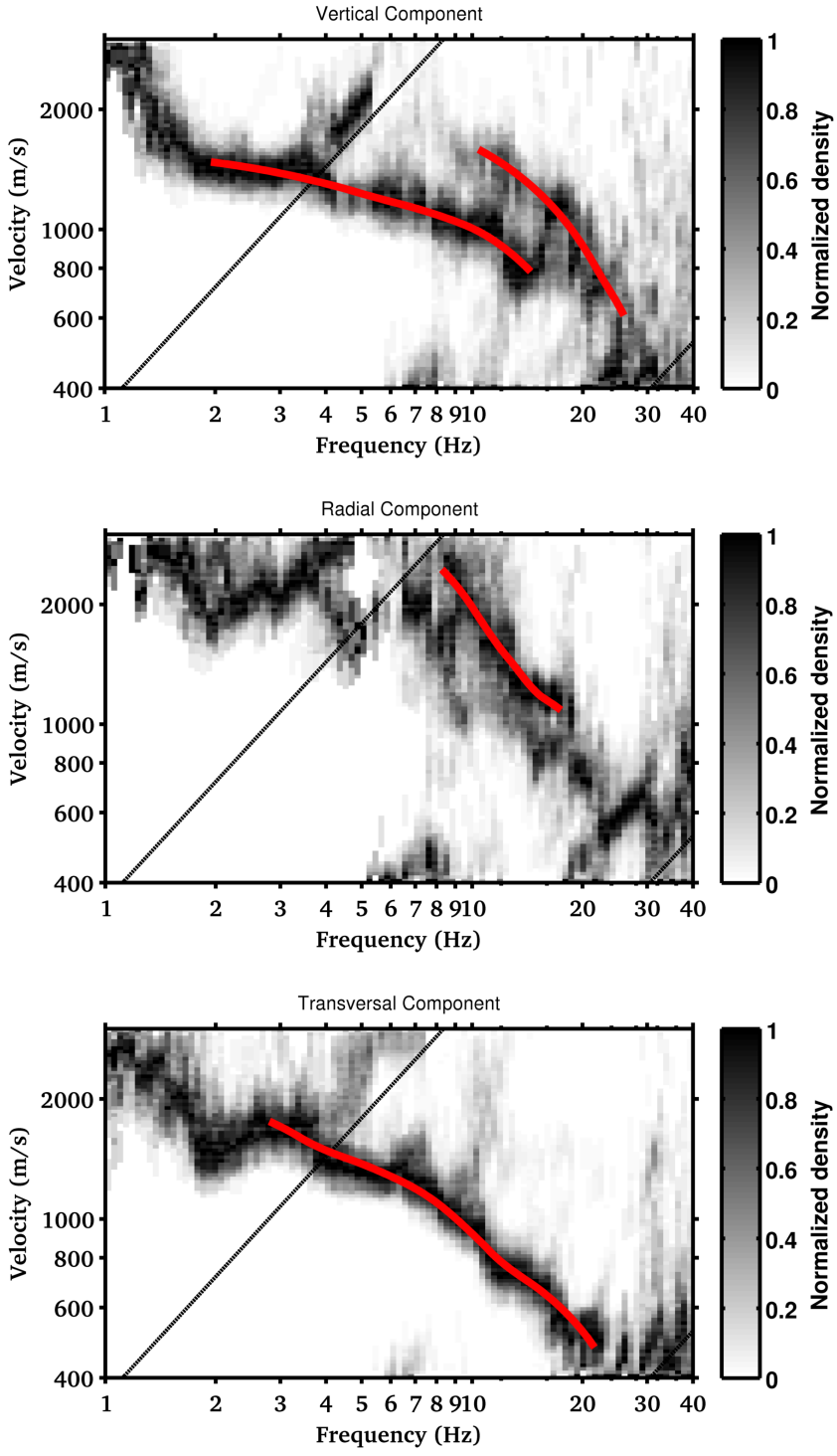

Figure 13 - *Density distribution of the surface wave signals obtained from the recording of the array configuration A2 using three-component f-k analysis. From top to bottom: Rayleigh vertical, Rayleigh radial and Love wave dispersion. In red the interpreted dispersion curves are given (manually selected).*

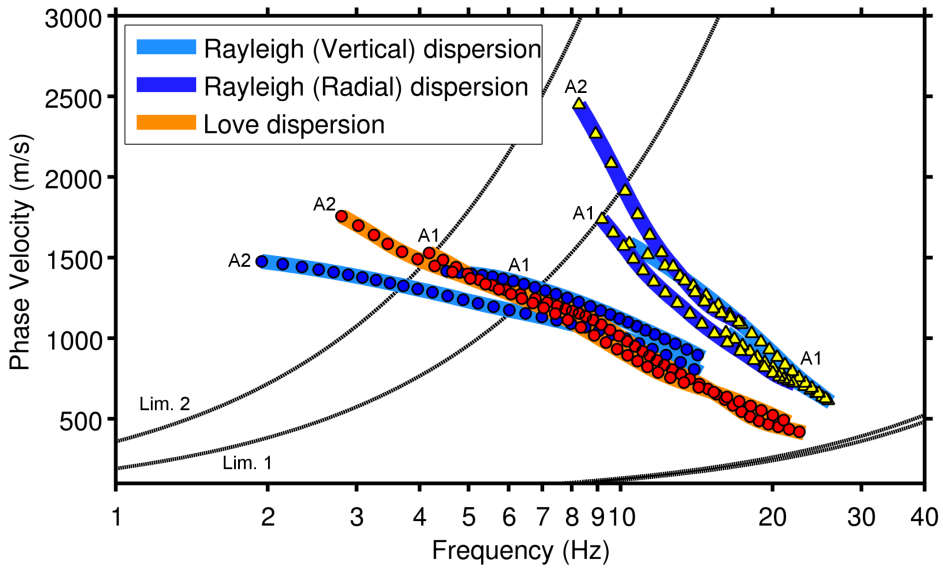

Figure 14 - *Summary of all dispersion curves obtained from three-component f-k analysis of the two array configurations A1 and A2. Minimum and maximum resolution bounds from the two geometries are indicated with black solid lines.*

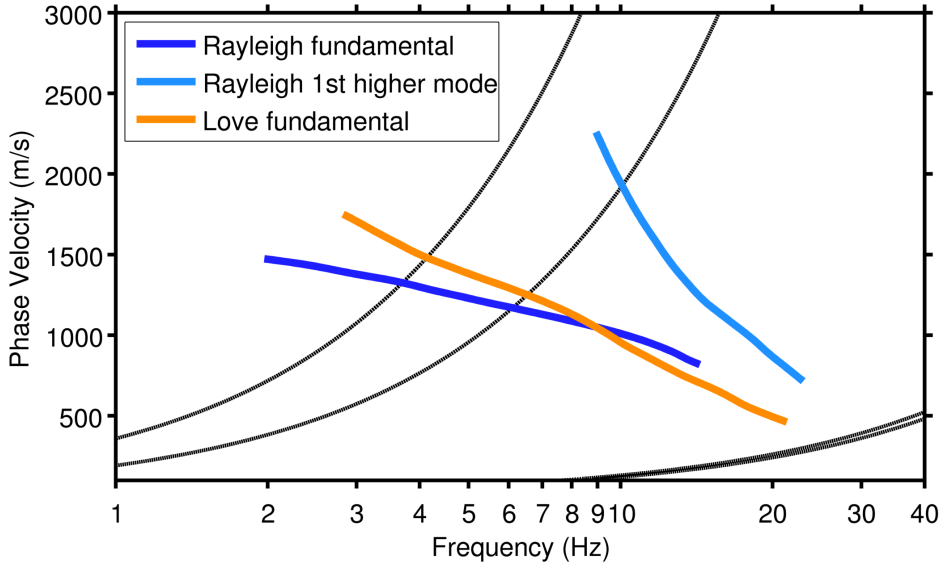

Figure 15 - *Final interpretation of the Rayleigh and Love dispersion curves for WALHA. Minimum and maximum resolution bounds from the full array are indicated with black solid lines.*

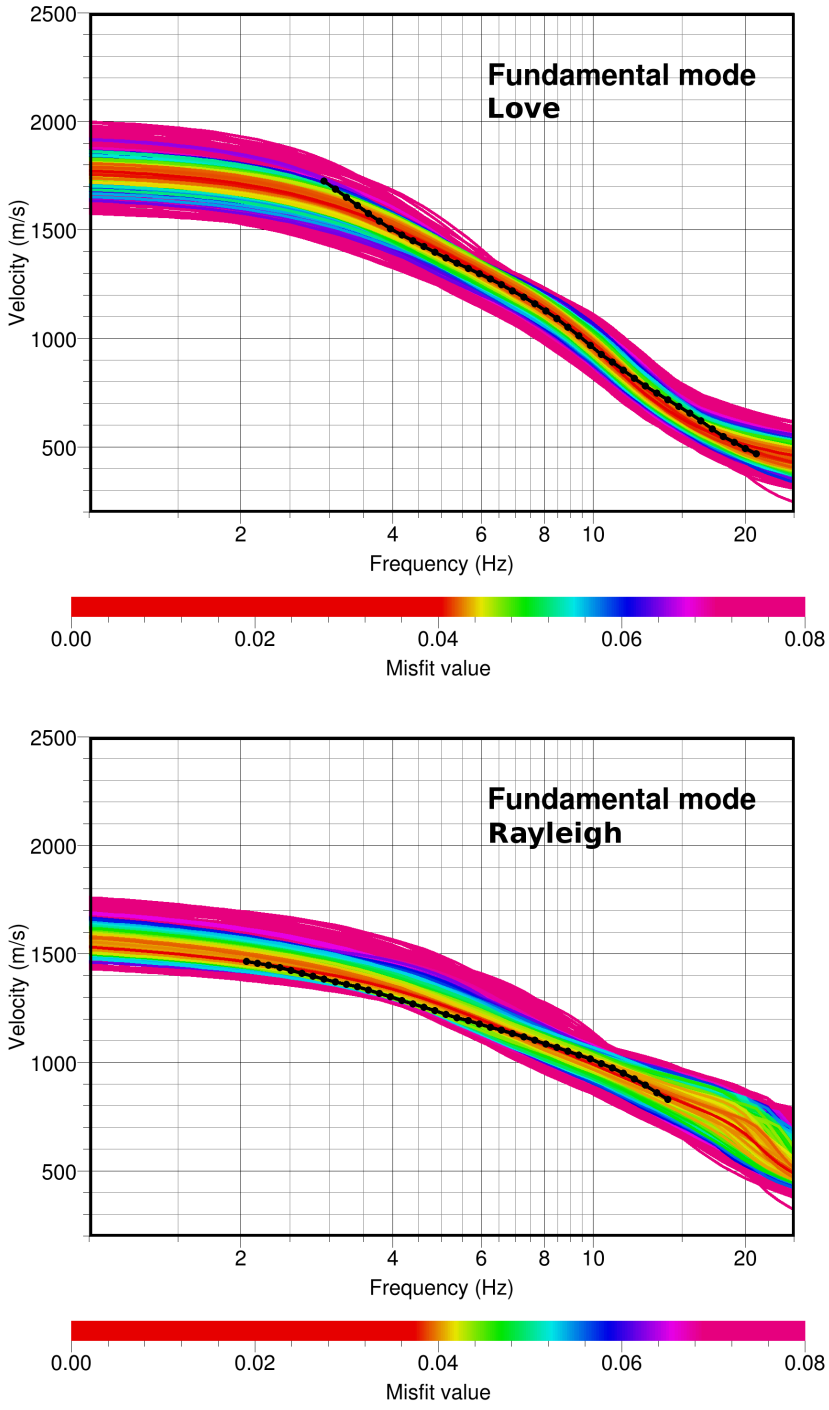

Figure 16 - *Fitting the surface dispersion data within the global optimization procedure; in this example, the Rayleigh and Love fundamental modes. Different colors represent different misfit between the observed (in black) and the modeled dispersion curves during the search.*

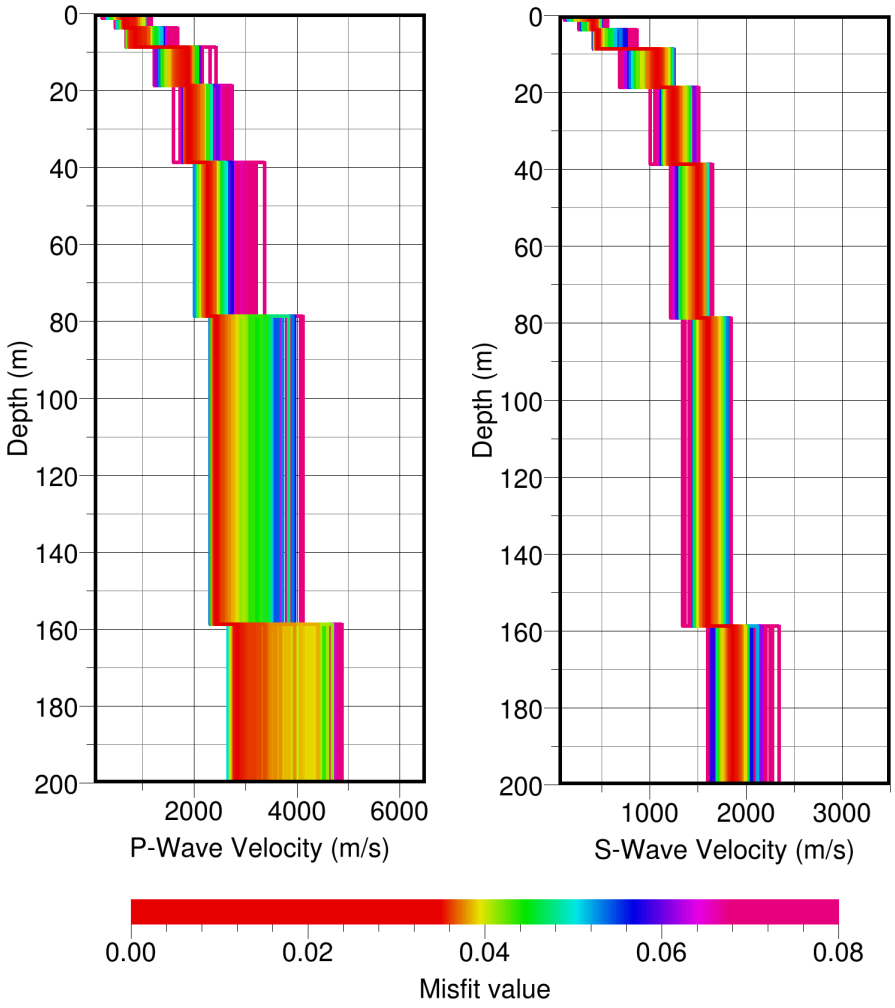

Figure 17 - *Distribution of the fix-layer velocity models generated during the inversion process and ordered by decreasing misfit, according to the color scheme of* **Figure 16**.

To parameterize the velocity model, two different approaches were implemented. The first one consisted in setting up an eight-layer model with fix interface depths (**Figure 17**). In such a case the free inversion parameters are then the velocities (P and S) and layer thicknesses. In the second case, a free-thickness layer approach was used (**Figure 18**). The advantage of the former method stays in the possibility to better resolve sharp velocity interfaces, while the second is less unique and better constraints the seismic velocity. The two approaches have to be nevertheless considered complementary, and they should provide consistent results. Ten inversion tests (*runs*) were performed for each of the two model schemes, in order to minimize the effect related to a possible unfavorable initial randomization of the parameter space. The best fitting model from of each run was then collected (**Figure 19** and **Figure 21**) and used later on for the computation of the derived soil parameters.

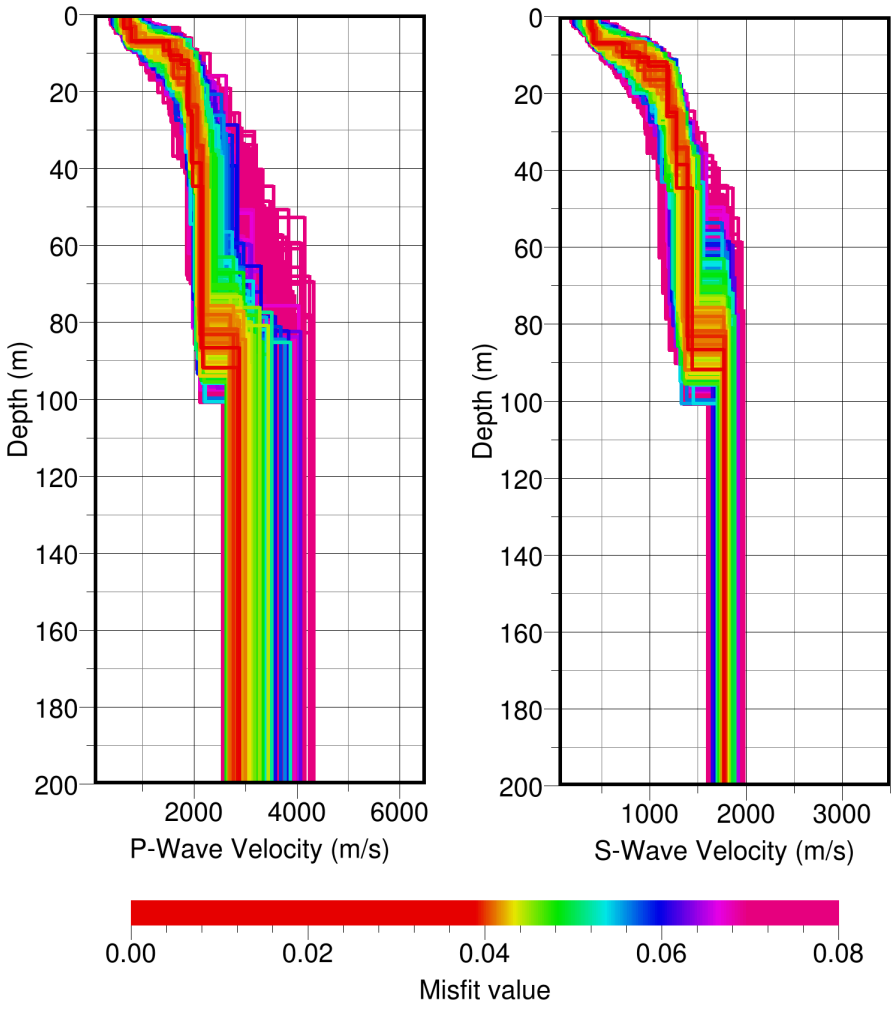

Figure 18 - *Distribution of the free-layer velocity models generated during the inversion process and ordered by decreasing misfit, according to the color scheme of* **Figure 16**.

In more detail, the inverted velocity models (Vs and Vp) are gradient-like, with a faster increase in velocity in the first 20m, followed by a smoother part. This is generally expected for a rock velocity profile. The uppermost velocities of the profile, however, are not directly constrained by the data (**Figure 20**), because of the lack of information at high frequencies, and might be underestimating the true values for the topmost 10m. By considering the minimum available frequency of the surface-wave dispersion curves, and by analyzing the scattering of the inverted models (**Figure 21**), it is realistic to assume the velocity profiles to be reliable down to a depth of about ~120m. Below this value no direct constrain is available from f-k analysis, and the velocity values are obtained by pure extrapolation.

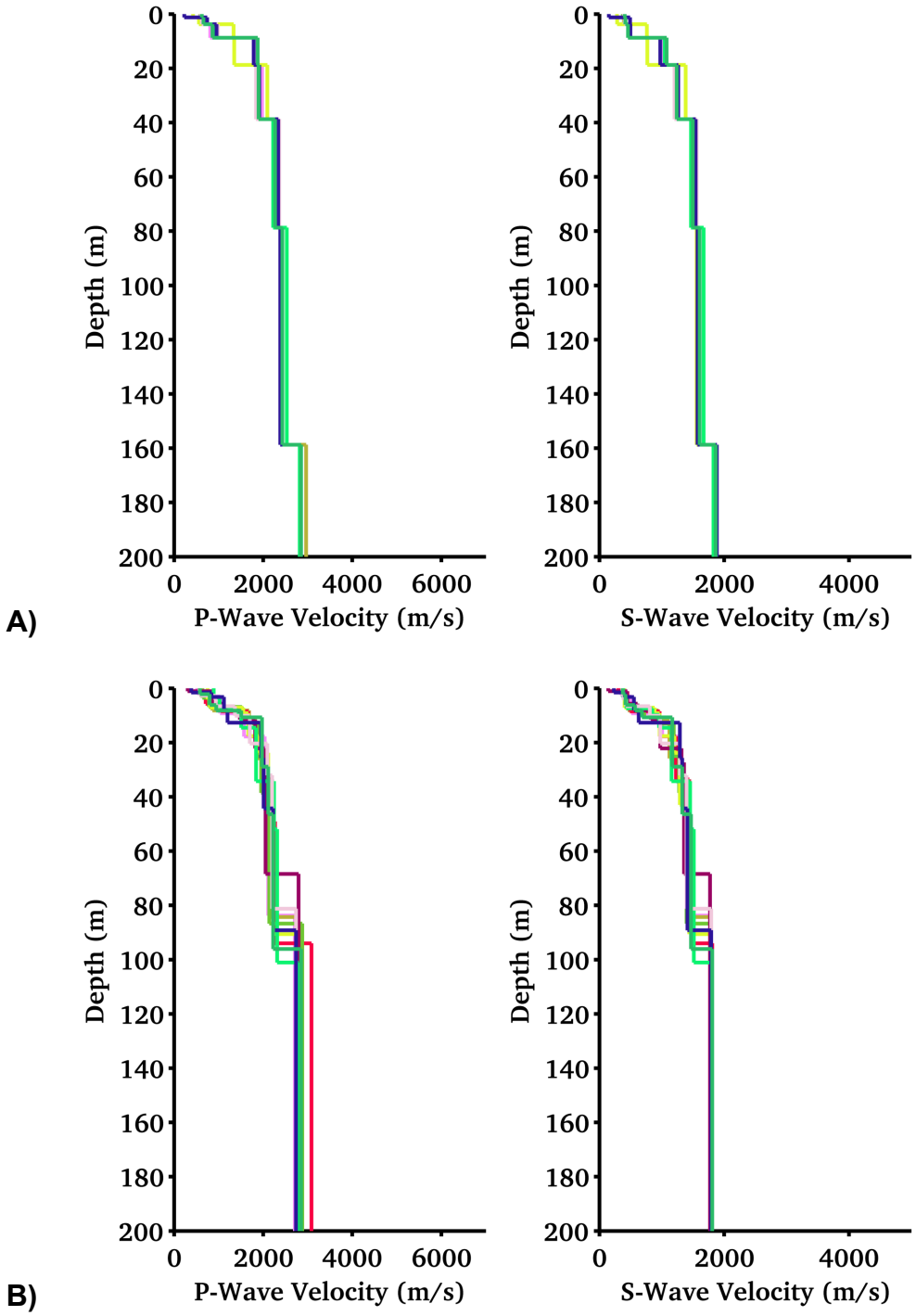

Figure 19 - *Collecting the best fitting models from the ten separated inversion runs using the free-layers (A, top) and fixed-layers (B, bottom) parameterization schemes.*

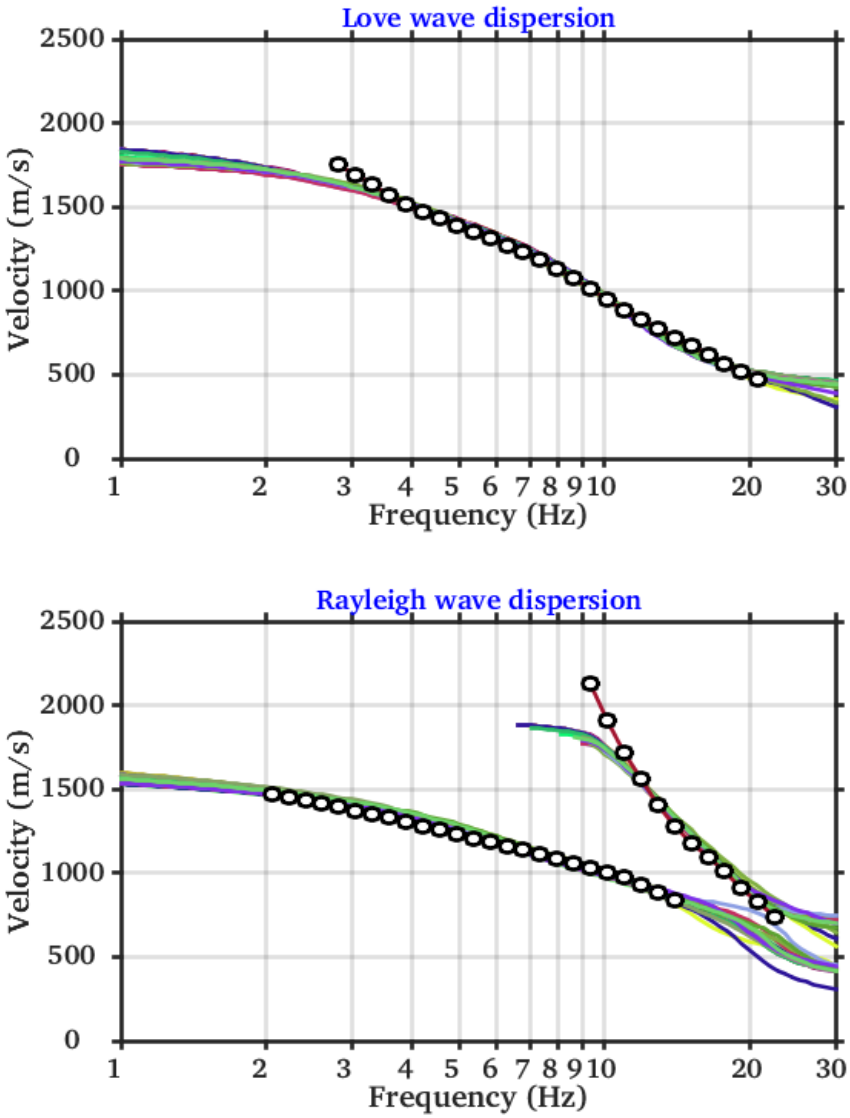

Figure 20 - *Rayleigh and Love dispersion curves computed from the 20 best fitting models of the two proposed interpretation schemes (free and fix layers). Fitting is good for both components, including the Rayleigh waves first overtone.*

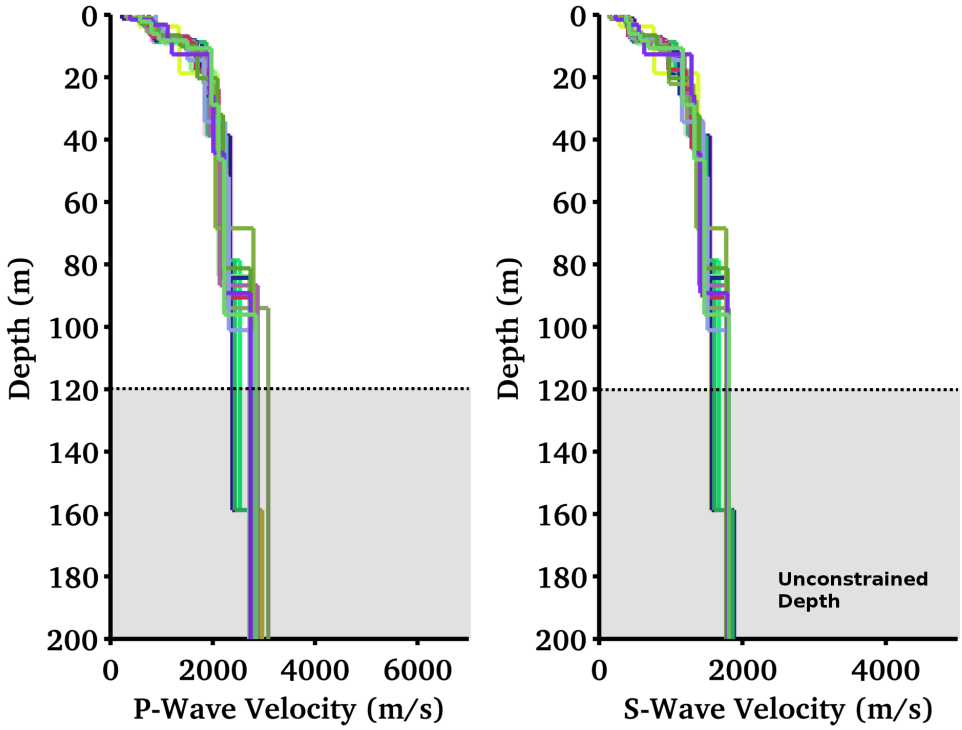

Figure 21 - *Comparison of all the best models from the two parameterization schemes (free and fixed layers). The two approaches produce consistent results. The depth of about 120m is considered approximately the maximum resolved depth.*

11. Engineering soil parameters

The ensemble of all the best inverted velocity profiles is then used to derive average soil parameters like the VsZ (average travel-time S-wave velocity over the depth Z, including Vs30, Table 1) and the quarter-wavelength (QWL) average velocities (Joyner et al., 1984) for a range of frequencies between 0.6 and 30Hz (**Figure 22**). The former is a standard parameter for the classification of ground-types in most building codes and in ground motion prediction equations. The latter is a parameter useful for the empirical estimation of the site-response and to assess the sensitivity of the seismic wave-field to the different depths. It has to be noticed that these two parameters are derived separately from all the best S-wave velocity models obtained from the inversion, and the results is finally averaged to improve statistics.

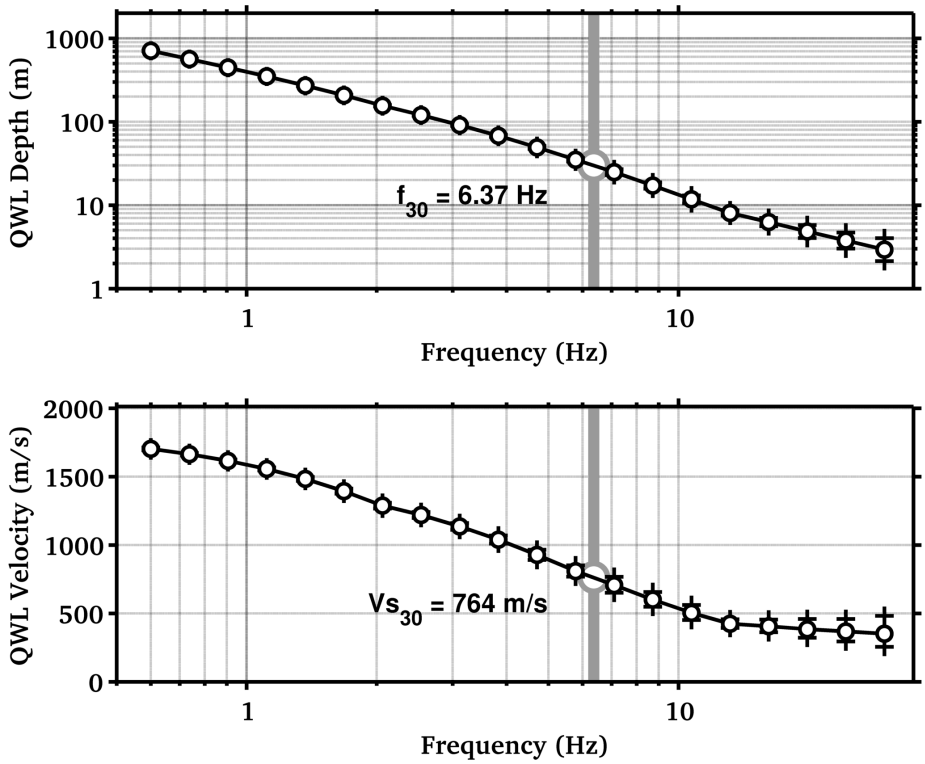

Figure 22 - *Quarter-wavelength representation of the inverted S-wave velocity profiles. Top: the depth-frequency dependency. Bottom: the QWL average velocity. The Vs30 value is indicated with its corresponding QWL frequency.*

12. Amplification models

Site amplification functions have been computed using two different approaches: the S-wave transfer function for vertical propagation and the quarter-wavelength amplification. In general the first method is used to evaluate the resonance characteristics of the site, while the second is more useful to assess the effect of the velocity contrasts between the lowermost rock layer (as reference) and the different QWL averaging depths. The two amplification functions are then corrected for the Swiss rock reference velocity profile as defined in Poggi et al. (2011), according to the procedure described in Edwards et al. (2013). Given the lower velocities in the uppermost part of the WALHA profile compared to the Swiss reference, the final corrected amplification function shows a lower average amplification level at high frequencies than the uncorrected (**Figure 23**).

Averaging depth (m)	Vs-mean (m/s)	St.Dev.
5	397.9305	38.9636
10	464.1567	21.22431
15	566.8519	26.29674
20	642.1789	30.5964
25	711.1462	28.47808
30	**766.062**	**26.13665**
40	851.3006	22.23505
50	933.7835	20.88589
75	1072.414	18.39015
100	1165.622	16.90059
150	1278.679	16.51862
200	1380.971	14.02402

Table 1 - *Average travel-time velocities at different depths. Vs30 is highlighted.*

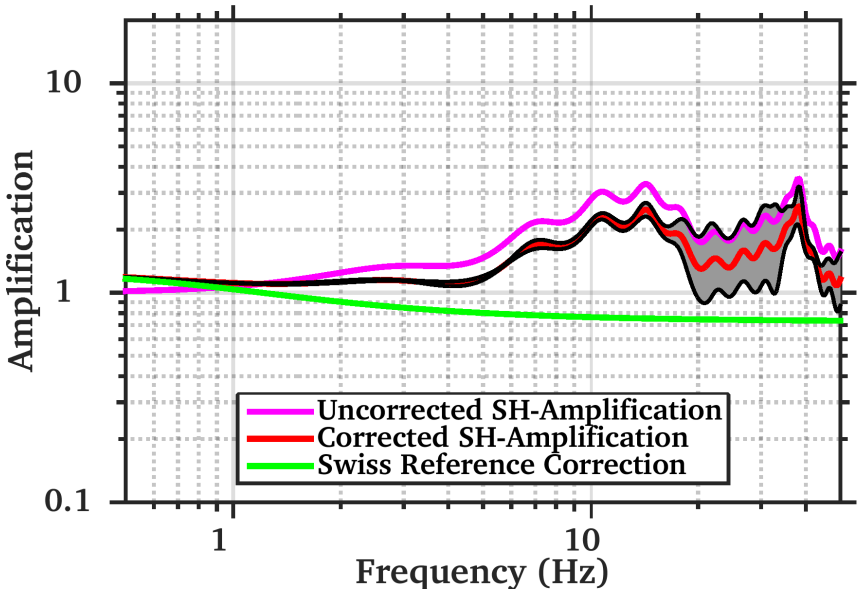

Figure 23 - *Correcting the SH-wave transfer function for the Swiss (rock) reference conditions (Poggi et al. 2011). The final corrected amplification function shows a lower (average) amplification at high frequencies than the uncorrected.*

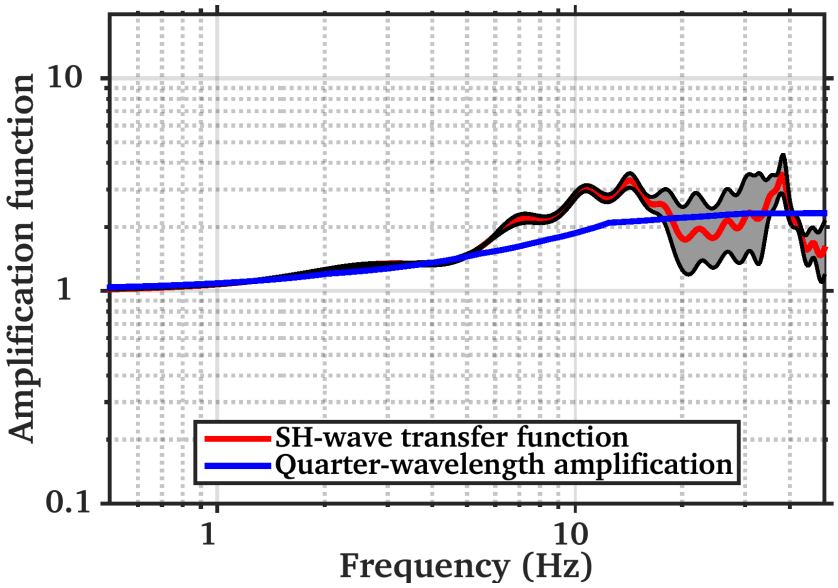

Figure 24 - *Comparison of amplification functions computed using the SH-wave transfer function and the quarter-wavelength formalism on the inverted velocity models.*

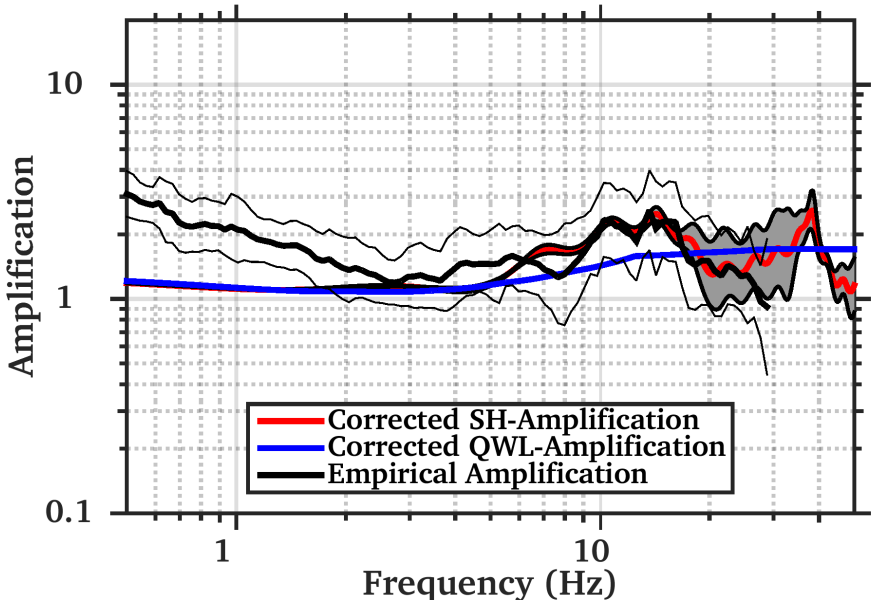

Figure 25 - *Comparison of amplification functions computed using the SH-wave transfer function and the quarter-wavelength approach with empirical observation from spectral modeling of low-magnitude earthquakes. All functions are referenced to the Swiss rock reference model (Poggi et al. 2011).*

Amplification functions using the transfer function and the quarter-wavelength approach are comparable (**Figure 24**), even if the transfer function provides a slightly larger amplification, because of the presence of some weak resonance peaks. At low frequencies both methods converge to the same amplification level. It has to be notice that the amplification functions do not include attenuation at this stage of the analysis, as the quality factors of the site are unknown.

A good matching is obtained by comparison between the one-dimensional transfer function and the empirical amplification from spectral modeling of low-magnitude earthquakes as described in Edwards et al., 2013 (**Figure 25**). Resonance peaks are mostly well reproduces by analytical solution, even though empirical amplification presents a positive shift at low frequency, which cannot be explained by the available data.

REFERENCES

Capon, J., 1969. High resolution frequency wavenumber spectrum analysis, Proc. IEEE, 57, 1408-1418.

Burjanek, J., G. Stamm, V. Poggi, J.R. Moore, and D. Fäh [2010], “Ambient vibration analysis of an unstable mountain slope”, Geophys. J. Int., Vol. 180, pp. 820-828.

Edwards, B., C. Michel, V. Poggi and D. Fäh (2013). Determination of Site Amplification from Regional Seismicity: Application to the Swiss National Seismic Networks. Accepted for publication in Seismological Research Letters.

Joyner, W. B., R. E. Warrick and T. E. Fumal (1981). The Effect of Quaternary Alluvium on Strong Ground Motion in the Coyote Lake, California, Earthquake of 1979, Bulletin of the Seismological Society of America, 71, 1333-1349.

Poggi, V., B. Edwards and D. Fäh (2011). Derivation of a Reference Shear-Wave Velocity Model from Empirical Site Amplification, Bulletin of the Seismological Society of America, 101, 258-274.

Poggi, V. and Fäh D., 2010. Estimating Rayleigh wave particle motion from three-component array analysis of ambient vibrations. Geophys. J. Int., 180-1, 251-267.